Terahertz Electro-Optic Sampling in Thick ZnTe Crystals Below the Reststrahlen Band With a Broadband Femtosecond Laser

Bang Wu, Lei Cao, Zhe Zhang, Qiang Fu, and Yongqian Xiong

***Abstract*—The method of electro-optic (EO) sampling of terahertz (THz) pulses in thick EO crystals leads to waveform distortions due to effects of phase mismatch, dispersive propagation, and absorption. In this paper, we demonstrate theoretically and experimentally that EO sampling with a broadband femtosecond (fs) laser could significantly eliminate these distortions below the Reststrahlen band. Our simulation results show that the oscillations and dips in the signals of EO response function of thick crystals are smoothed out by the broadband spectrum of the femtosecond laser. In the experiment, we use a laser with a bandwidth of 100 nm and a low temperature GaAs photoconductive antenna to generate typical THz pulses (0.1–3 THz). The measurement results confirm that a $\langle 110 \rangle$-oriented 3-mm-thick ZnTe crystal is an attractive EO material for sampling THz pulse below 3 THz and agree with simulation results. This technique is particularly useful in areas where a large time window is needed, for example in the THz time-domain spectroscopy system.**

***Index Terms*—Broadband laser, electro-optic (EO) sampling, terahertz (THz), thick crystals.**

I. Introduction

THE electro-optic (EO) sampling technique has been widely used in terahertz (THz) time-domain spectroscopy (THz-TDS) thanks to its high spectral resolution and sensitivity [1], [2]. Besides the ability to characterize the temporal waveform of a THz pulse, the THz-TDS method based on EO samplings can also accurately determine the complex dielectric constant of materials, and find increasing applications in nondestructive detection [3], [4], biological and medical research [5]–[7], advanced materials research [8], [9], as well as in other fields of spectroscopy [10]. Moreover, it is a powerful tool for the study of ultrafast processes such as, carrier dynamics [11]–[14], phonon dynamics [15], [16], ultrashort electron bunches profiles [17], [18], the monitor of THz pulse from laser plasma [19], free-electron lasers [20], and other THz sources [21]. The measured EO signal should be a replica of the THz pulse. However, it is distorted due to the phase mismatch in the electro-optic process, dispersive propagation, and absorption of the THz pulse in EO crystals [22], [23]. These distortion effects become more severe with the increase of crystal thickness, and hence an appropriate thin crystal is usually employed. Nevertheless, the Fabry–Perot effect (multiple reflections) occurring in thin crystals will restrict the length of detection time window and therefore, limit the improvement of the spectroscopy resolution. Meanwhile echoes mixed with the original signals can further distort the detected THz pulse.

To overcome these disadvantages in thin crystals, several material processing methods were proposed to eliminate the Fabry–Perot effect but they cannot completely solve the problem. The approach of THz antireflection coating [24]–[26] was suggested, while the non-negligible imaginary optical conductivity of the coating materials introduces considerable losses. The use of a wedge-shaped EO crystal is a practical method [27], but the THz pulse should be carefully focused to a size of small spot. Meanwhile, a few numerical echo cancellation methods based on deconvolution algorithms [28]–[30] have been recommended, although these methods strongly depend on the assumed dispersion models of the EO crystal or a careful calibration of the reference signal.

In comparison with thin crystals, EO sampling with thick crystals has higher detected signal intensity as well as a large time window suitable in spectroscopy applications without any addition material processing. However, thick crystals suffer from signal distortions. Previous studies on the distortion effects of thick EO crystals are based on the assumption that the bandwidth $\Delta\omega$ of probe laser is only a small fraction of the center frequency, i.e., $\Delta\omega/\omega_0 \ll 1$ [22], [23], [31]–[33]. If a broadband probe pulse is used, the frequency-dependent EO process becomes more complicated, and the broadband spectrum of probe pulse may play a positive role on alleviating these distortions. Kampfrath *et al*. [34] found that at frequencies above the Reststrahlen band, the phase-mismatch-induced oscillations in thick crystals could be smoothed by a 10-fs sampling laser pulse. For example, a 250-μm-thick ZnTe crystal has equivalent detection efficiency as a 10-μm-thin crystal at the frequency above 10 THz [34].

In this paper, we demonstrate that a very thick crystal can be used in EO sampling of a THz pulse below the Reststrahlen band ($<$5.3 THz for ZnTe) with the help of a broadband femtosecond

Manuscript received December 18, 2017; accepted February 16, 2018. Date of publication March 19, 2018; date of current version May 1, 2018. This work was supported in part by National Natural Science Foundation of China under Grant 61705071 and in part by the "2011 project" organized by the Hubei Collaboration Innovation Center of Non-power Nuclear Technology. *(Corresponding authors: Lei Cao and Yongqian Xiong.)*

The authors are with the State Key Laboratory of Advanced Electromagnetic Engineering and Technology, Huazhong University of Science and Technology, Wuhan 430074, China (e-mail: wubang@hust.edu.cn; leicao@hust.edu.cn; zhzhang@hust.edu.cn; qfu@hust.edu.cn; yqxiong@hust.edu.cn).

Color versions of one or more of the figures in this paper are available online at http://ieeexplore.ieee.org.

Digital Object Identifier 10.1109/TTHZ.2018.2810018

(fs) laser. In Section II, we briefly describe the EO sampling process and show theoretically that how the distortion effects of EO crystals can be smoothed out by the broadband spectrum of the probe laser. Experiments are conducted to verify that a 3-mm-thick ZnTe crystal shows attractive detection performances at frequencies below the Reststrahlen band with a broadband (FWHM = 100 nm) femtosecond (fs) laser in Section III. Finally, the summary and potential applications of this technique are given in Section IV.

II. Theoretical Models and Simulation Results

A. Theoretical Models

In the detection of THz pulses by EO sampling, the fs optical pulse overlaps with the THz pulse in EO crystals. The polarization of the fs pulse is rotated by the THz electric field through Pockels effect, and the polarization change can be measured by ellipsometry with a quarter wave plate (QWP) and a Wollaston polarizer. A detailed principle description of EO sampling technique of THz pulses can be found in [35].

In the frequency domain, the detected EO sampling signal $S(\Omega)$ can be expressed as the product of the EO response function $f(\Omega)$ and the incident THz electric field $E_{\mathrm{THz}}(\Omega)$ [35]

$$S(\Omega) = \frac{\pi \in_0}{c} f(\Omega) E_{\mathrm{THz}}(\Omega) \tag{1}$$

where ϵ_0 is the vacuum permittivity and c is the light speed in vacuum.

Following the approach in [35], the EO response function $f(\Omega)$ is derived from the coherent addition of the sum- and difference-frequency components generated through mixing of THz and optical signals

$$f(\Omega) = \int_{-\infty}^{+\infty} C(\omega,\Omega) P(\omega,\Omega) T_{\mathrm{THz}} T_{\mathrm{opt}} A^*(\omega) A(\omega-\Omega) d\omega. \tag{2}$$

The response function behaves as a spectral filter which takes into account the frequency-dependent phase match factor

$$P(\omega,\Omega) = [e^{i\Delta k(\omega,\Omega) l} - 1]/i\Delta k(\omega,\Omega) \tag{3}$$

the nonlinear coupling coefficient between the THz and probe pulses

$$C(\omega,\Omega) = \omega^2 \chi^{(2)}(\omega-\Omega,\Omega)/k_r \tag{4}$$

the amplitude transmission coefficient of the THz pulse $T_{\mathrm{THz}}(\Omega) = 2/(1+2n_{\mathrm{THz}}(\Omega))$, and the power transmittivity of the probe pulse $T_{\mathrm{opt}}(\omega) = (4n(\omega)/(1+n(\omega))^2)^2 \exp(-2\beta(\omega) l)$ [34], [35]. Here, l is the thickness of the nonlinear crystal, $\chi^{(2)}$ is the second-order dielectric susceptibility, and $A(\omega)$ is the spectrum of the probe laser at the incident side of the EO crystal. The variables $k_r(\omega)$ and $\beta(\omega)$ are the corresponding real and imaginary parts of the complex wavenumber $k(\omega) = k_r(\omega) + i\beta(\omega)$, where $\beta(\omega)$ reflects the optical frequency losses of the probe laser propagating through the crystal. $n_{\mathrm{THz}}(\Omega)$ and $n(\omega)$ are the corresponding refractive index of the crystal in THz and optic frequency range.

The complex wavenumber mismatch between the optical and THz frequencies is considered in the expression $\Delta k(\omega,\Omega) = k(\omega-\Omega) + k(\Omega) - k(\omega)$. The real part of $\Delta k(\omega,\Omega)$ describes the mismatch of phase and group velocities between the THz and probe laser pulses, whereas the imaginary part of $\Delta k(\omega,\Omega)$ represents the usual strong absorption of the THz pulse in the EO crystal. We keep the expansion of $k_r(\omega)$ to the second order so as to consider the effect of group velocity dispersion (GVD) of the fs probe laser pulse in the crystal

$$k_r(\omega) = k_r(\omega_0) + (\omega-\omega_0) k_{r1}(\omega_0) + 1/2(\omega-\omega_0)^2 k_{r2}(\omega_0) \tag{5}$$

where $k_{r1}(\omega_0) = \frac{dk_r(\omega)}{d\omega}|_{\omega=\omega_0}$ and $k_{r2}(\omega_0) = \frac{d^2 k_r(\omega)}{d\omega^2}|_{\omega=\omega_0}$.

Therefore, the real part of $\Delta k(\omega,\Omega)$ can be expressed by

$$\Delta k_r(\omega,\Omega) = k_r(\Omega) - \Omega k_{r1}(\omega_0) + \frac{1}{2}[\Omega^2 - 2(\omega-\omega_0)\Omega] k_{r2}(\omega_0). \tag{6}$$

Under the limit condition, if the bandwidth of probe pulse is much smaller than the carrier frequency ($\omega \approx \omega_0$), the approximation expression for the EO response function is simplified as

$$f(\Omega) = C(\omega_0) P(\omega_0,\Omega) T_{\mathrm{THz}} T_{\mathrm{opt}} C_{\mathrm{opt}} \tag{7}$$

where $C_{\mathrm{opt}}(\Omega) = \int_{-\infty}^{+\infty} A^*(\omega) A(\omega-\Omega) d\omega$ is the autocorrelation function of the probe pulse. If we assume a Gaussian beam profile of the probe laser with narrow bandwidth, this function will reduce to $C_{\mathrm{opt}}(\Omega) \propto \tau_p \exp\{-[\tau_p/2\ln(2)]^2 \Omega^2/4\}$, which contains explicitly the pulse duration at FWHM (τ_p). But for the broadband probe laser, the general form of the response function (2) should be used.

B. Simulation Results

In order to study and explain the EO process in thick crystals with a broadband fs laser, we consider the EO response function of ZnTe crystal and perform a theoretical calculation to retrieve the real THz pulse.

In the calculation, we assume a Gaussian distribution of the probe pulse, and the laser spectrum is determined by its bandwidth ($\lambda_0 = 800$ nm, $\Delta\lambda = \mathrm{FWHM} = 100$ nm). The condition of narrowband ($\omega \approx \omega_0$, $\Delta\lambda = 10$ nm) probe laser is also included in the calculation for comparison purposes. The general expression (2) and its approximate form (7) are utilized for the calculation of response functions for the broadband and narrowband laser pulse, respectively. The complex refractive index and second-order dielectric susceptibility of the ZnTe crystal are taken from [31].

Figs. 1 and 2 show the calculated amplitude and phase of the response function of ZnTe crystals, respectively, under narrowband approximation [See Figs. 1(a) and 2(a)] and with a broadband fs laser [See Figs. 1(b) and 2(b)] at various thicknesses. For a narrowband probe laser, the EO response function follows the tendency as reported in [31]. As the crystal thickness increases, the amplitude of the response function increases. In particular, when the thickness reaches 3 mm, severe amplitude dips appear due to the phase mismatch. At these frequencies (0.95 and 2.05 THz for the 3-mm-thick crystal), the phase of the response function undergoes abrupt change as shown in

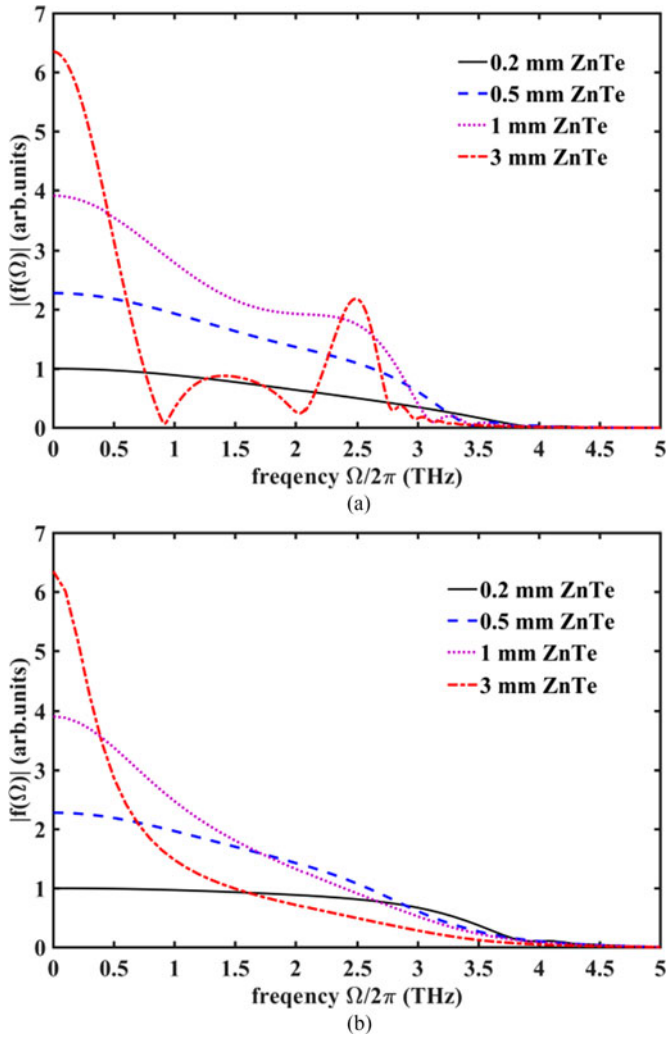

Fig. 1. Amplitude of the ZnTe response function for (a) a 10-nm narrowband laser and (b) a 100-nm broadband laser with a crystal thickness of 0.2, 0.5, 1, and 3 mm. For clarity, the response functions are normalized to the maximum value of the response function of the 0.2-mm-thick ZnTe.

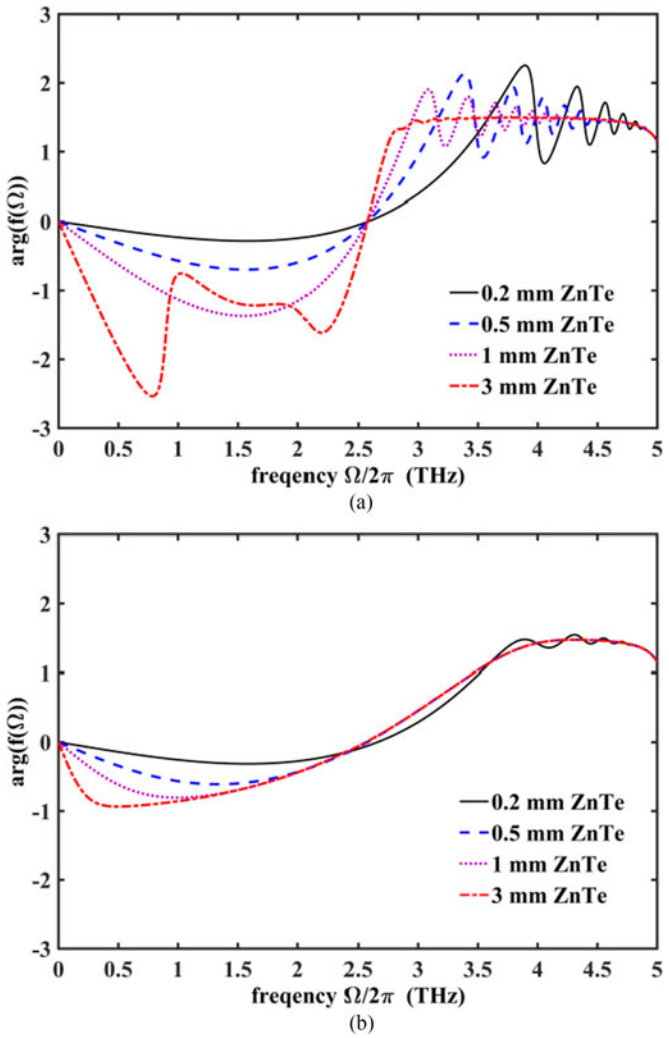

Fig. 2. Phase of the ZnTe response function for (a) a 10-nm narrowband laser and (b) a 100-nm broadband laser with a crystal thickness of 0.2, 0.5, 1, and 3 mm.

Fig. 2(a), which indicates the probe pulse walks off the THz field from a positive half-wave to the negative half yielding a tiny EO signal. For the probe laser with a 100-nm bandwidth in the simulation, these amplitude dips disappear and accordingly a flat phase diagram is obtained in Fig. 2(b). This signifies that the phase mismatch, absorption, and other filtering effects are smoothed out by the broadband laser spectrum in the integration (2). Particularly, in the frequency range between 1 and 3 THz, the response function of a 3-mm-thick ZnTe crystal is much smooth than that of the standard 1-mm-thick crystal. But for the frequency below 1 THz, the response function falls quickly, which will filter the THz spectra.

The Fourier transform of (1) is performed to reconstruct the time domain EO signal. For simplicity, a bipolar waveform incident THz pulse is assumed ($E_{\mathrm{THz}}(t) = -t/T\exp(-t^2/T^2)$) and the constant $T = 200$ fs was selected to be consistent with experiment conditions in the Section III. The retrieved time domain EO signals and their frequency domain spectra are shown correspondingly in Figs. 3 and 4 with narrowband [See Figs. 3(a) and 4(a)] and broadband probe lasers [See Figs. 3(b) and 4(b)]. In both cases if the thin crystal (0.2 mm) is adopted the retrieved waveform is similar with the incident pulse. For thicker crystals (>0.2 mm), detection with a broadband probe laser (100 nm) owns its advantages.

With a narrowband probe laser, obvious oscillation tail arises in the EO signal when the crystal thickness is higher than 0.2 mm [See Fig. 3(a)]. For example, strong oscillations in the EO signal of the 3-mm-thick crystal contribute to the local maximum at 2.46 THz in its spectrum [See Fig. 4(a)]. The results are in accordance with the analysis and experimental observations in [22]. If a 3-mm-thick ZnTe crystal is used, the EO signal is strongly modulated by the response function and severely distorted with respect to the incident THz pulse. The peak-to-peak time interval augments from 0.28 ps (incident pulse) to 1.10 ps (3 mm ZnTe) and the amplitude of oscillation tail becomes comparable with the main THz signal. The Fourier-transformed spectra of the EO pulses in Fig. 4(a) clearly demonstrate a force modification in the frequency domain (the 0.95- and 2.05-THz dips and the 2.46-THz local maximum) by a 3-mm-thick ZnTe crystal.

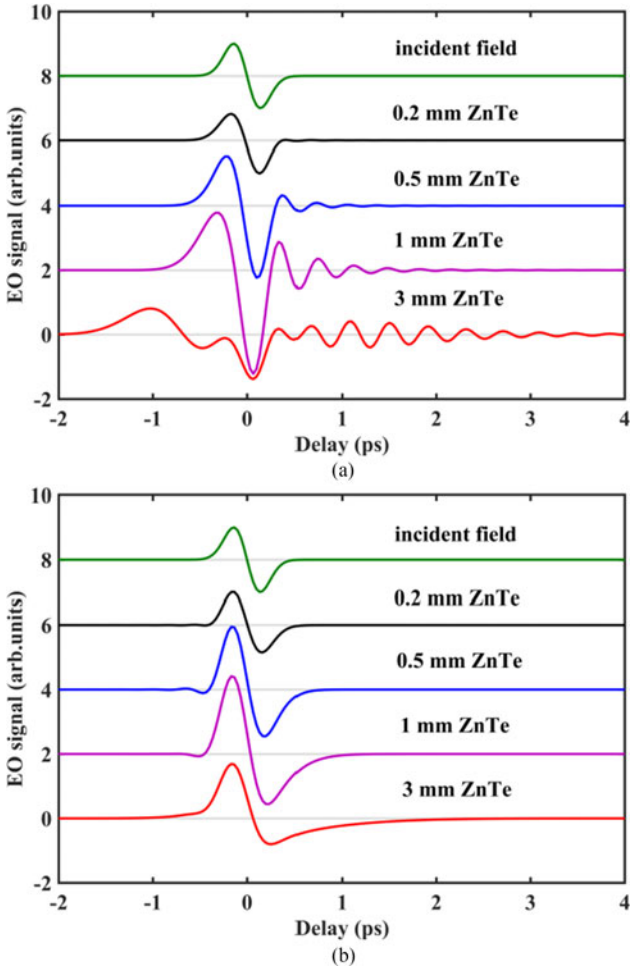

Fig. 3. Calculated EO signals for four ZnTe crystals of different thicknesses with (a) a 10-nm narrowband laser and (b) a 100-nm broadband laser.

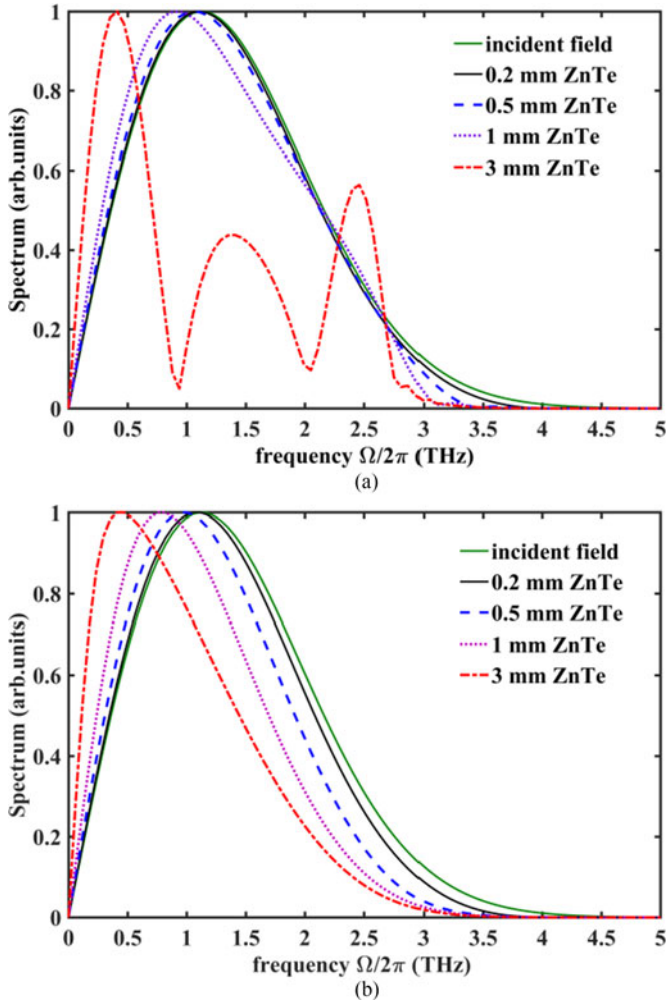

Fig. 4. Calculated spectra of the THz EO signal for four ZnTe crystals of different thicknesses with (a) a 10-nm narrowband laser and (b) a 100-nm broadband laser.

For a probe laser with a bandwidth of 100 nm shown in Fig. 3(b), no oscillation tails appear at different crystal thicknesses. With the increase of crystal thickness from 0.2 to 3 mm, the positive half pulse waveform experiences no evident change and the peak-to-peak time interval is enlarged slightly from 0.3 to 0.4 ps. However, it should be note that the amplitude of the negative half pulse reduces significantly by 53% and the pulse width broadens from 0.26 to 0.56 ps. This effect results in the band narrowing in the THz spectrum as shown in Fig. 4(b). The FWHM bandwidth reduces from 1.72 THz (0.2-mm-thick crystal) to 1.37 THz (3-mm-thick crystal). And the calculated spectrum with the 3-mm-thick crystal has an evident frequency redshift of 0.64 THz in reference to the 0.2-mm case. Due to the power absorption of the fs probe pulse and the filter effect below 1 THz of the incident THz pulse in thick crystals, the maximum EO signal of the 3-mm-thick crystal is only 1.7 times (not 15 times) that of the 0.2-mm-thick crystal.

III. Experimental Results and Discussions

To verify the calculation results, an EO sampling experiment with a 10-fs laser and ZnTe crystals at different thicknesses was designed and performed.

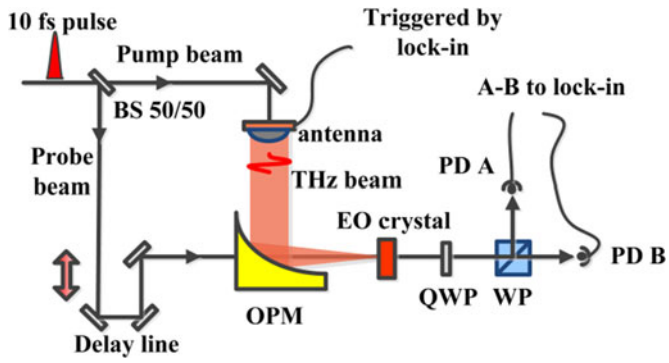

Fig. 5. Experimental setup for EO sampling of THz pulses. BS–beam splitter, OPM–off-axis parabolic mirror, QWP–quarter-wave plate, WP–Wollaston prism, PD–photodiode.

A. Experimental Results

The measurement setup is schematically shown in Fig. 5. A Ti:Sapphire laser oscillator (Femtolasers Synergy) with a pulse duration of 10-fs, a pulse energy 6.6 nJ, a central wavelength of 800 nm, a bandwidth of 100 nm, a repetition rate of 79.33 MHz,

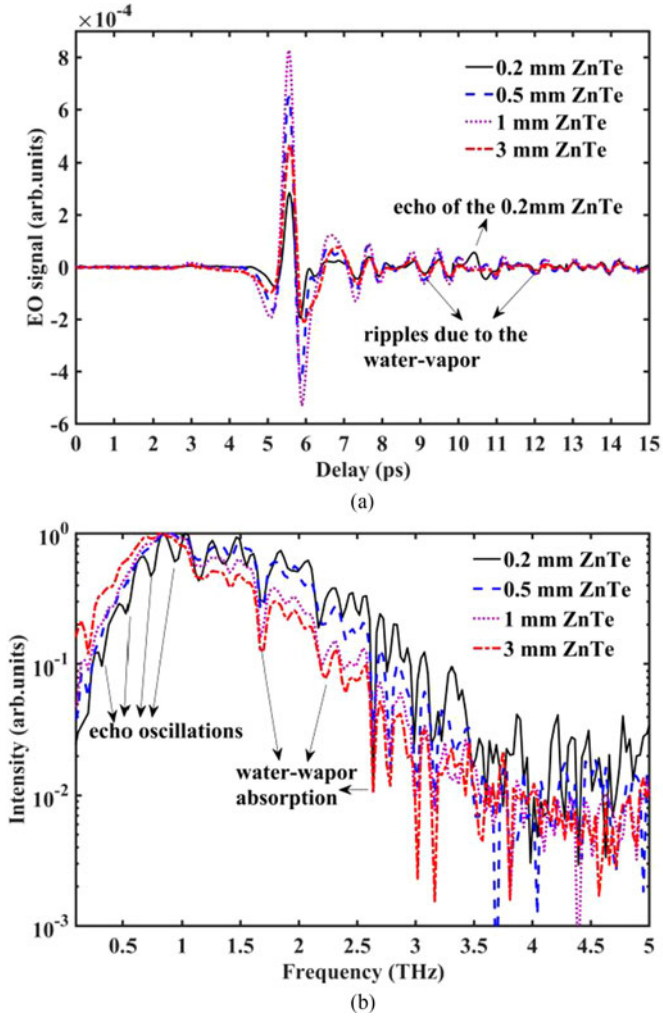

Fig. 6. (a) EO detected signal of ZnTe crystals with different thicknesses. For clarity, the time origin is shifted. (b) Spectra of the measured THz EO signal. Note the EO signals of all the crystals have the same residual ripples after the main EO signal due to the dispersion and absorption in water vapor, which result in the dips higher than 1 THz in the spectrum.

and an average power of 600 mW is used. The fs pulse splits into pump and probe beams with a power ratio of 50/50. The pump beam is used to excite the low temperature GaAs photoconductive antenna (gap $= 5\ \mu$m), which generates THz pulses in the range of 0.1–3 THz. Then, the THz beam and the probe beam are both focused collinearly onto a $\langle 110 \rangle$-oriented ZnTe crystal. Inside the EO crystal, the THz electric field rotates the polarization of the probe beam through Pockels effect. The polarization change of probe laser is measured by a standard balanced detection method combining a QWP that turns linear polarization probe laser into a distorted circular polarization and a Wollaston prism which splits both polarization components. A balanced photodiode (PD) detector is used to measure the intensity change which is proportional to the THz electric field. The temporal waveform of the THz field is obtained by scanning the optical delay between the THz and probe pulses.

The detected EO signals with four ZnTe crystals at different thicknesses are shown in Fig. 6(a). An echo signal at a time interval of $\Delta t = 4.83$ ps from the main pulse is the reflected THz signal at the back surface of the 0.2-mm-thick ZnTe crystal ($\Delta t = 2nd/c$, n is the refractive index of the ZnTe crystal, and $d = 0.2$ mm is its thickness). This will restrict the sampling time window which determines the spectral resolution in a THz-TDS system. As the crystal thickness increases to 1 mm or even 3 mm, it is surprising that no evident distortions arise and the oscillatory tail in EO signals frequently observed due to the dispersive propagation of THz pulse in thick crystals disappear (the residual ripple after the main EO signal is caused by the dispersion and absorption in water vapor). However, the negative half of temporal THz pulse is slightly broadened by thick crystals, resulting in a narrowing of the corresponding spectrum, as shown in Fig. 6(b). For instance, the peak-to-peak time interval is enlarged from 0.3 to 0.4 ps as the crystal thickness increase from 0.2 to 3 mm, and FWHM of the negative peak broadens from 0.2 to 0.5 ps at the same time, leading to the diminution of the corresponding spectrum bandwidth (FWHM) from 1.5 to 0.7 THz. This observed phenomenon is different from the case when the THz frequency is above the Reststrahlen band, where the spectrum measured by a thicker crystal slightly broadens than the thinner one [34]. Compared with the 0.2-mm-thick crystal, spectrum measured with the 3-mm-thick crystal has a frequency redshift about 0.1 THz. If influences of water vapor are excluded from the experiment, larger frequency redshift should appear.

B. Discussions

The detected maximum EO signal of the 3-mm-thick crystal is about 1.6 times that of the 0.2-mm-thick ZnTe crystal. Although this signal is lower than that of the 0.5 or 1 mm thick crystal, the signal-to-noise ratio (SNR) is almost at the same level. In the experiment, the SNR augments from 230 to 510 as the thickness of crystal increases from 0.2 to 1 mm, and then reduces slightly to 420 when the thickness increases to 3 mm. Actually, due to the absorption in thick ZnTe, the power transmittivity of the fs pulse in 3-mm ZnTe crystal is about 50% of that in 1-mm crystal and 42% of that in 0.2-mm crystal. Therefore, if we increase the fs laser output power to keep the power absorbed by the PD at the same level with different crystal thicknesses, the SNR value of thick crystals could be probably enhanced.

In accordance with the theoretical calculations with narrowband and broadband lasers, in the experiment with a 3-mm-thick crystal, the EO signal spectrum dips (0.95 and 2.05 THz) due to the mismatch of the phase and group velocities of the THz and probe pulse are not observed. Additionally, the oscillatory tails in the frequency range between 2 and 3 THz due to the dispersive propagation of THz pulse in thick crystal disappear. Moreover, as shown in Fig. 6(b), when the spectrum is calculated from the time-domain data including the secondary echo in the 0.2 mm ZnTe crystal, the spurious etalon oscillations arise apparently. Such oscillations interfere in data analysis and may obscure important features in the absorption spectrum. When the thickness of crystals increases from 0.2 to 3 mm, the echo interval Δt increases accordingly from 4.83 to 72.5 ps, which means the spectral resolution can be increased by 15 times without etalon oscillations.

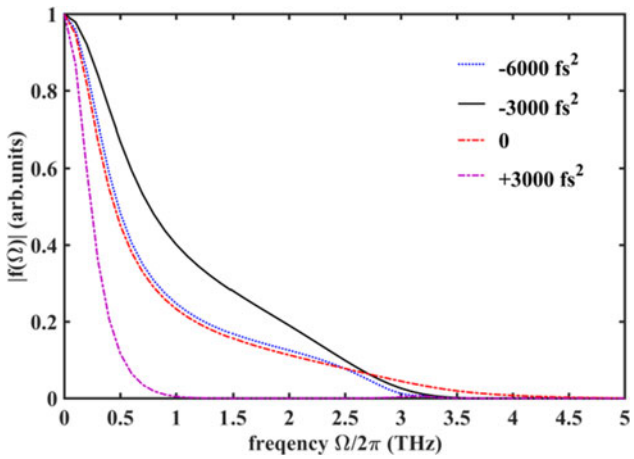

Fig. 7. Calculated response functions for the 3-mm-thick ZnTe crystal with a 10-fs 100-nm broadband laser at difference initial GDD. For clarity, the response functions are normalized to the maximum of that at zero initial GDD.

When the broadband laser pulse propagates through the thick EO crystal, the group velocity dispersion (GVD $= k_{r2}(\omega_0)$) will broaden the temporal profile of the pulse. The pulse duration τ_p (FWHM) grows with increasing depth in the EO crystal $\tau_p(l) = \sqrt{\tau_{\mathrm{p0}}^2 + (k_{r2}(\omega_0)l)^2 \tau_{\mathrm{p0}}^{-2}}$, where τ_{p0} is the incident pulse duration. The calculated GVD value of the ZnTe crystal shows that a 3-mm-thick ZnTe will add a group delay dispersion (GDD $= k_{r2}(\omega_0)l$) of $+6000\,\mathrm{fs}^2$ to the laser pulse at the center wavelength of 800 nm. This means that a 10-fs pulse will broaden to 600 fs after propagating through the 3-mm crystal. The obvious probe pulse broadening effect is one of the main reasons why the EO signal amplitude drops in the 3-mm-thick crystal in both the simulation and experiment results. In practice, one could alleviate this effect on EO signals by using a negatively prechirped probe pulses to achieve optimal compression of the pulse in the middle of the EO crystal [36]. Similar to the treatment of the phase mismatch factor Δk, we include an expansion of the phase of the incident probe laser spectrum $A(\omega)$ to its second order to account for the initial GDD. The simulated response function of the 3-mm-thick ZnTe with different initial GDD is shown in Fig 7. A -3000-fs^2 prechirped probe pulse is preferred to obviously enhance the detected EO signal intensity.

The experiment results are in agreement with our simulations and show that the distortions by thick crystal in EO processes are smoothed by the broadband spectrum of the probe laser. Also, it should be noted that the smoothing effect may also exists in other kinds of EO materials, such as organic EO crystals [37]. Moreover, this technique could be applied in single-shot EO detection schemes, such as transverse-spatial encoding [38], pulse front tilting [39], and reflective echelons [40].

IV. Conclusion

In conclusion, we present a detailed theoretical analysis and calculation of the EO sampling process below Reststrahlen band, and show that a broadband laser can significantly eliminate the distortions caused by phase mismatch, dispersive propagation, and absorption in thick crystals. When a 100-nm bandwidth fs laser is applied in EO sampling with a 3-mm-thick ZnTe crystal, the oscillatory tail in the frequency range between 2 and 3 THz due to the dispersive propagation and the dips in THz spectrum at 0.95 and 2.05 THz due to the phase mismatch disappear. In the time domain, the main positive pulse waveform and the peak-to-peak time interval are almost invariant. However, the negative pulse waveform broadens along with the decrease of amplitude and results in a band narrowing and redshift in the THz spectrum.

We experimentally demonstrated that for the frequency below 3 THz, a ZnTe crystal as thick as 3 mm can be used for THz pulse characterization without remarkable distortions, especially for the main positive pulse. The response amplitude of the EO signal of a 3-mm-thick ZnTe crystal is about 1.6 times as high as that of a 0.2-mm-thick crystal. As predicted by the calculation results, the phenomena of band narrowing and frequency redshift in the THz spectrum due to the broadened negative pulse are also observed, which is different from the phenomenon observed previously above the Reststrahlen band. We believe that the technique of distortion elimination in thick crystals by a broadband fs laser will be very useful when a large time window is needed in a THz-TDS system, as well as in some single-shot THz EO detection configurations.

Acknowledgment

The authors would like to thank S. K. Zhang at Jefferson Lab for helpful discussion on the electro-optic sampling.

References

[1] Q. Wu and X.-C. Zhang, "Free-space electro-optic sampling of terahertz beams," *Appl. Phys. Lett.*, vol. 67, no. 24, pp. 3523–3525, Oct. 1995.
[2] B. Urbanek *et al.*, "Femtosecond terahertz time-domain spectroscopy at 36 kHz scan rate using an acousto-optic delay," *Appl. Phys. Lett.*, vol. 108, Mar. 2016. Art. no. 121101.
[3] M. Theuer, S. S. Harsha, D. Molter, G. Torosyan, and R. Beigang, "Terahertz time-domain spectroscopy of gases, liquids, and solids," *Chem. Phys. Chem.*, vol. 12, no. 15, pp. 2695–2705, Jul. 2011.
[4] K. Kawase, Y. Ogawa, Y. Watanabe, and H. Inoue, "Nondestructive terahertz imaging of illicit drugs using spectral fingerprints," *Opt. Express*, vol. 11, no. 20, pp. 2549–2554, Oct. 2003.
[5] I. Amenabar, F. Lopez, and A. Mendikute, "In introductory review to THz nondestructive testing of composite mater," *J. Infrared Millim. THz Waves*, vol. 34, no. 2, pp. 152–169, Feb. 2013.
[6] M. Nedvedova, V. Kresalek, Z. Adamik, and I. Provaznik, "Terahertz time-domain spectroscopy for studying absorbable hemostats," *IEEE Trans. THz Sci. Technol.*, vol. 6, no. 3, pp. 420–426, May 2016.
[7] N. Chopra, K. Yang, Q. H. Abbasi, K. A. Qaraqe, M. Philpott, and A. Alomainy, "THz time-domain spectroscopy of human skin tissue for in-body nanonetworks," *IEEE Trans. THz Sci. Technol.*, vol. 6, no. 6, pp. 803–809, Nov. 2016.
[8] C. Koral, B. Ortaç, and H. Altan, "Terahertz time-domain study of silver nanoparticles synthesized by laser ablation in organic liquid," *IEEE Trans. THz Sci. Technol.*, vol. 6, no. 4, pp. 525–531, Jul. 2016.
[9] G. P. Papari, V. Gargiulo, M. Alfè, R. D. Capua, A. Pezzella, and A. Andreone, "THz spectroscopy on graphene-like materials for biocompatible devices," *J. Appl. Phys.*, vol. 121, Apr. 2017, Art. no. 145107.
[10] G. J. Wilmink and J. E. Grundt, "Current state of research on biological effects of terahertz radiation," *J. Infrared Millim. THz Waves*, vol. 32, no. 10, pp. 1074–1122, Oct. 2011.
[11] R. Ulbricht, E. Hendry, J. Shan, T. F. Heinz, and M. Bonn, "Carrier dynamics in semiconductors studied with time-resolved terahertz spectroscopy," *Rev. Mod. Phys.*, vol. 83, no. 2, pp. 543–586, Jun. 2011.
[12] A. Rubano, M. Wolf, and T. Kampfrath, "Terahertz conductivity and ultrafast dynamics of photoinduced charge carriers in intrinsic 3C and 6H silicon carbide," *Appl. Phys. Lett.*, vol. 105, Jul. 2014, Art. no. 032104.

[13] L. Braun *et al.*, "Ultrafast photocurrents at the surface of the three-dimensional topological insulator Bi2Se3," *Nat. Commun.*, vol. 7, Oct. 2016, Art. no. 13259.
[14] Y. Minami, J. Takeda, T. D. Dao, T. Nagao, M. Kitajima, and I. Katayama, "Nonlinear electron dynamics of gold ultrathin films induced by intense terahertz waves," *Appl. Phys. Lett.*, vol. 105, Dec. 2014, Art. no. 241107.
[15] T. Kampfrath, L. Perfetti, F. Schapper, C. Frischkorn, and M. Wolf, "Strongly coupled optical phonons in the ultrafast dynamics of the electronic energy and current relaxation in graphite," *Phys. Rev. Lett.*, vol. 95, Oct. 2005, Art. no. 187403.
[16] Y. Ikegaya, H. Sakaibara, Y. Minami, I. Katayama, and J. Takeda, "Real-time observation of phonon-polariton dynamics in ferroelectric LiNbO3 in time-frequency space," *Appl. Phys. Lett.*, vol. 107, Aug. 2015, Art. no. 062901.
[17] G. Berden, S. P. Jamison, A. M. MacLeod, W. A. Gillespie, B. Redlich, and A. F. G. van der Meer, "Electro-optic technique with improved time resolution for real-time, nondestructive, single-shot measurements of femtosecond electron bunch profiles," *Phys. Rev. Lett.*, vol. 93, Sep. 2004, Art. no. 114802.
[18] G. Berden *et al.*, "Benchmarking of electro-optic monitors for femtosecond electron bunches," *Phys. Rev. Lett.*, vol. 99, Oct. 2007, Art. no. 164801.
[19] Y. Minami, T. Kurihara, K. Yamaguchi, M. Nakajima, and T. Suemoto, "Longitudinal terahertz wave generation from an air plasma filament induced by a femtosecond laser," *Appl. Phys. Lett.*, vol. 102, Apr. 2013, Art. no. 151106.
[20] G. M. H. Knippels *et al.*, "Generation and complete electric-field characterization of intense ultrashort tunable far-infrared laser pulses," *Phys. Rev. Lett.*, vol. 83, no. 8, pp. 1578–1581, Aug. 1999.
[21] T. Seifert *et al.*, "Ultrabroadband single-cycle terahertz pulses with peak fields of 300 kV cm^{-1} from a metallic spintronic emitter," *Appl. Phys. Lett.*, vol. 110, Jun. 2017, Art. no. 252402.
[22] H. J. Bakker, G. C. Cho, H. Kurz, Q. Wu, and X.-C. Zhang, "Distortion of terahertz pulses in electro-optic sampling," *J. Opt. Soc. Amer. B, Opt. Phys.*, vol. 15, no. 6, pp. 1795–1801, Jun. 1998.
[23] J. Faure, J. Van Tilborg, R. A. Kaindl, and W. P. Leemans, "Modeling laser-based table-top THz sources: Optical rectification, propagation, and electro-optic sampling," *Opt. Quant. Electron.*, vol. 36, no. 8, pp. 681–697, Jun. 2004.
[24] A. Thoman, A. Kern, H. Helm, and M. Walther, "Nanostructured gold-films broadband terahertz antireflection coatings," *Phys. Rev. B, Condens. Matter*, vol. 77, May 2008, Art. no. 195495.
[25] L. Ding *et al.*, "Ultrathin film broadband terahertz antireflection coating based on impedance matching method," *IEEE J. Sel. Top. Quant.*, vol. 23, no. 4, pp. 1–8, Jul. 2017.
[26] J. Kröll, J. Darmo, and K. Unterrainer, "Metallic wave-impedance matching layers for broadband terahertz optical systems," *Opt. Express*, vol. 15, no. 11, pp. 6552–6560, May 2007.
[27] B. Steffen *et al.*, "Electro-optic time profile monitors for femtosecond electron bunches at the soft x-ray free-electron laser FLASH," *Phys. Rev. Special Topics, Accel. Beams*, vol. 12, Mar. 2009, Art. no. 032802.
[28] J. R. Fletcher, G. P. Swifta, D.-C. Dai, and J. M. Chamberlain, "Pulsed terahertz signal reconstruction," *J. Appl. Phys.*, vol. 102, Dec. 2007, Art. no. 113105.
[29] M. Naftaly and R. E. Miles, "A method for removing etalon oscillations from THz time-domain spectra," *Opt. Commun.*, vol. 280, no. 2, pp. 291–295, Dec. 2007.
[30] A. Redo-Sanchez and X.-C. Zhang, "Self-referenced method for terahertz wave time-domain spectroscopy," *Opt. Lett.*, vol. 36, no. 17, pp. 3308–3310, Sep. 2011.
[31] S. Casalbuoni, H. Schlarb, B. Schmidt, P. Schmüser, B. Steffen, and A. Winter, "Numerical studies on the electro-optic detection of femtosecond electron bunches," *Phys. Rev. Special Topics, Accel. Beams*, vol. 11, Jul. 2008, Art. no. 072802.
[32] A. Tomasino *et al.*, "Wideband THz time domain spectroscopy based on optical rectification and electro-optic sampling," *Sci. Rep.*, vol 3, Oct. 2013, Art. no. 3116.
[33] O. Kenichi, O. Makoto, and S. Watanabe, "Retrieving the undistorted terahertz time-domain electric-field vector from the electro-optic effect," *J. Opt. Soc. Amer. B, Opt. Phys.*, vol. 34, no. 9, pp. 1946–1956, Sep. 2017.
[34] T. Kampfrath, J. Nötzold, and M. Wolf, "Sampling of broadband terahertz pulses with thick electro-optic crystals," *Appl. Phys. Lett.*, vol. 90, Jun. 2007, Art. no. 231113.
[35] G. Gallot and D. Grischkowsky, "Electro-optic detection of terahertz radiation," *J. Opt. Soc. Amer. B, Opt. Phys.*, vol. 16, no. 8, pp. 1204–1212, Aug. 1999.
[36] D. N. Erschens, D. Turchinovich, and P. U. Jepsen, "Optimized optical rectification and electro-optic sampling in ZnTe crystals with chirped femtosecond laser pulses," *J. Infrared Millim. THz Waves*, vol. 32, no. 12, pp. 1371–1381, Sep. 2011.
[37] T. Taniuchi, S. Okada, and H. Nakanishi, "Widely tunable terahertz-wave generation in an organic crystal and its spectroscopic application," *J. Appl. Phys.*, vol. 95, May 2004, Art. no. 5984.
[38] J. Shan *et al.*, "Single-shot measurement of terahertz electromagnetic pulses by use of electro-optic sampling," *Opt. Lett.*, vol. 25, no. 6, pp. 426–428, Mar. 2000.
[39] Y. Kawada, T. Yasuda, A. Nakanishi, H. Takahashi, and S. Aoshima, "Single-shot measurement of terahertz temporal waveform using pulse-front tilting by a direct vision dispersion prism," *Rev. Sci. Instrum.*, vol. 80, Nov. 2009, Art. no. 113703.
[40] Y. Minami, Y. Hayashi, J. Takeda, and I. Katayama, "Single-shot measurement of a terahertz electric-field waveform using a reflective echelon mirror," *Appl. Phys. Lett.*, vol. 103, Jul. 2013, Art. no. 051103.

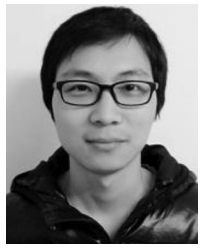

Bang Wu received the B.S. degree from the College of Physics, Huazhong University of Science and Technology, Wuhan, China, in 2012. He is currently working toward the Ph.D. degree at the School of Electrical and Electronic Engineering, Huazhong University of Science and Technology, Wuhan, China.

His main research interests include time-domain spectroscopy and free electron lasers.

Lei Cao received the B.Eng. degree in electronics information and M.Eng. degree in electromagnetic field and microwave technology from the Huazhong University of Science and Technology, Wuhan, China, in 2007 and 2009, respectively, and the Ph.D. degree in physics from the Institut d'Electronique Fondamentale, Université Paris Sud, France, in 2013.

From May 2013, he is a Lecturer with the State Key Laboratory of Advanced Electromagnetic Engineering and Technology, Huazhong University of Science and Technology. His current research interests include the characterization of free electron laser (FEL) type terahertz (THz) radiation sources, field effect transistor (FET) type THz detectors, and planar THz waveguides.

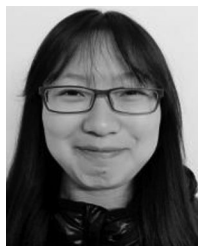

Zhe Zhang received the B.S. degree from the College of Physics, Huazhong University of Science and Technology, Wuhan, China, in 2012. She is currently working toward the Ph.D. degree at the School of Electrical and Electronic Engineering, Huazhong University of Science and Technology.

Her main research interests include plasma-surface interaction and terahertz detectors.

Qiang Fu received the B.S. degree from the College of Physics, Huazhong University of Science and Technology, Wuhan, China, in 2011. He is currently working toward the Ph.D. degree at the School of Electrical and Electronic Engineering, Huazhong University of Science and Technology.

His research focuses on free electron lasers.

Yongqian Xiong received the Ph.D. degree in Electric Machinery from the Huazhong University of Science and Technology, Wuhan, China, in 1995.

He is a Professor with the School of Electrical and Electronic Engineering, Huazhong University of Science and Technology. His research efforts have been concentrated in the areas of electric machines and free electron laser-based terahertz sources.